Impact of ultra-thin-layer material parameters on the suppression of carrier injection in rectifying junctions formed by interfacial charge layers

Tihomir Knežević[1*], Tomislav Suligoj[1], and Lis K. Nanver[2]

[1]University of Zagreb, Faculty of Electrical Engineering and Computing, Micro and Nano Electronics Laboratory, Croatia

[2]University of Twente, Faculty of Electrical Engineering Mathematics & Computer Science, Enschede, The Netherlands

[*]tihomir.knezevic@fer.hr

Abstract - Pure amorphous boron (PureB) deposition on Si is used to fabricate ultrashallow low-saturation-current p⁺n-like diodes even at process temperatures where the boron is not expected to diffuse into the bulk Si. It has been proposed that the bonding of the B atoms to the Si creates a monolayer of fixed negative charge that attracts holes to the interface. In this paper, an investigation using semiconductor simulation tools is performed starting from an all-Si test structure where suppression of electron injection from an n-Si bulk was achieved by introducing a large concentration of negative fixed charge that attracts holes to the interface between a thin-film top-layer and the bulk. This introduces a barrier which lowers the electron saturation current density of the simulated diode to become comparable to or lower than the saturation current density of holes injected into the bulk. The material properties of the top-layer such as electron mobility and tunneling mass, bandgap and electron affinity are individually varied from default Si-values to values typical for amorphous boron layers indicating that a critical concentration of negative fixed charge is always needed for suppression of the electron injection.

Keywords – pure amorphous boron, PureB, negative fixed interface charge, carrier injection, ultra-thin-layer, TCAD

I. INTRODUCTION

In advanced CMOS and other nanoscale silicon device technologies, the fabrication of junctions with appropriately shallow junction depths, low leakage current and low series resistance, remains challenging. Monolayers could be used as a doping-source activated by thermal [1] or laser [2] annealing which inevitably increases the junction depth. Thus the fabricated diodes then function as conventional p-n diodes. In contrast, a pure boron layer (PureB) deposited in an anode region on the Si provides attractive p⁺n-like diode characteristics that are comparable to those of conventional deep junctions, albeit for junction depths of only a few nanometer. To our knowledge, the so-called PureB technology is the only example of diode fabrication with deposited dopant atoms where these are not driven into the Si. Depositions down to 250°C using chemical-vapor deposition (CVD) or down to 400°C using molecular beam epitaxy (MBE) offer back-end-of-the-line (BEOL) CMOS compatibility for fabrication of photodiodes [3], [4].

In addition to the electron blocking power that such a layer would give, PureB diodes fabricated as photodiodes with PureB-only light-entrance windows have also shown a very high stability with respect to high-dose irradiation with beams such as extreme-ultraviolet (EUV) light and low-energy electrons that carry so much energy with them that they readily degrade oxide interfaces. This, together with the nm-shallow distance to the radiation sensitive Si layer, has led to a rapid commercialization of PureB detectors for monitoring low-penetration depth beams such as those used in advanced lithography and electron microscopy systems [5], [6], applications for which also PureB single-photon avalanche diode (SPAD) detectors with low dark count rate [7] are under development.

At present, the physical mechanism behind the attractive PureB diode behavior still needs to be fully understood. Based on extensive experimental material, it has been proposed that a monolayer of acceptor states formed at the interface by B-to-Si bonds, is responsible for creating a layer of fixed negative charge that can maintain an interfacial hole layer [3], [8], [9]. Measurements have confirmed that the conductance along the PureB-Si interface is high even for deposition at 400°C where no doping of the bulk Si is expected [10]. From bipolar transistor measurements with PureB emitters, it was concluded that the concentration of holes at the interface would have to be larger than 10^{14} cm⁻² to be able to explain the very low base current, i.e., very high electron blocking power [9].

Most of the PureB material parameters are not well-known while material parameters of other boron layer depositions may vary depending on the fabrication method. To understand the impact that a negative interface charge has on the *I-V* characteristics of the fabricated diodes, we have already modeled PureB devices assuming an all-Si test structure. Suppression of the electron injection from bulk was achieved by assuming a large concentration of negative fixed charge between the Si top-layer and the bulk [3]. In this work, we vary the material properties of the top-layer such as mobility of electrons, bandgap and electron affinity to values typical for amorphous boron layers. A critical concentration of negative fixed charge is always

found to be necessary to explain the rectifying junctions formed by interfacial charge layers.

II. Material Properties of Amorphous Boron

Amorphous boron is a semiconducting material whose bandgap can significantly vary depending on the exact processing conditions. Hydrogenated amorphous boron films reported in [11] have an optical bandgap in the range between 1.4 eV and 1.7 eV with photoconductivity as low as 10^{-9} S/cm. These bandgap values are consistent with the values reported in [12] where the hydrogenated amorphous boron films were heat treated at 400°C for 200 hr which caused a decrease of the optical bandgap from 2.19 eV to 0.9 eV. The decrease of the bandgap is attributed to the reduction of the hydrogen content in the films [12].

Amorphous boron films prepared with different deposition techniques consistently showed lower bandgap than that of Si with variations in the measured value. The electrical bandgap of boron films grown by MBE was found to be 0.6 eV as measured by the electrical conductivity method [13]. Kuhlmann et al. [14] reported an optical bandgap of $\approx$ 0.75 eV for the several μm thick amorphous boron evaporated films. Electron-beam deposited amorphous boron films with thicknesses between 100 nm and 200 nm showed optical bandgaps of 0.5 eV [15]. Due to the presence of crystallization during the deposition of the amorphous layers, the bandgap could increase to values specific for a more ordered system such as α-rhombohedral boron or β-rhombohedral boron which have optical bandgaps of 2 eV and 1.6 eV, respectively [16]. This was also observed in [17] where the optical bandgap increased from 1.05 eV to 1.4 eV with an increase of the deposition temperature from 700°C to 900°C. One source also reported a thermal bandgap of bulk amorphous boron of 1.3 eV which is higher than that of Si [18].

The conductivity of the amorphous boron layers was found to be in the range from 10^{-3} S/cm to 10^{-5} S/cm at room temperature [13], [18]–[21]. Mobility and conductivity measurements identified that the majority carriers in the amorphous boron layers are holes [19]–[21]. This was also confirmed by scanning tunneling microscope (STM) measurement of a B-complex at the Si surface that places the Fermi level near the valence band edge [22] which is characteristic of p-type doped semiconductors. The values of conductivity, mobility and doping concentrations that have been measured for amorphous boron material in various sources are listed here:

- Boron films grown by MBE had a conductivity at 300 K of 1.5×10^{-5} S/cm [13]. The thermal dependence of the conductivity measured for the material [13] showed a $\log(\sigma)$ versus $T^{-1/4}$ behavior characteristic of the Mott's variable range hopping (VRH) conduction [23].

- The solid source molecular beam deposited films described in [19] had a conductivity in the range from $\approx$ 10^{-3} S/cm to $\approx$ 10^{-4} S/cm for growth temperatures between 200°C and 800°C, respectively. The measured drift mobility at room temperature was approximately 10 cm²/Vs while the concentration of holes was very low to be consistent with the measured low conductivity and ranged from 5.5×10^{15} cm^{-3} to 3.5×10^{13} cm^{-3}.

- Golikova showed an increase of the conductivity at room temperature from 1.6×10^{-6} S/cm to 10^{-3} S/cm for bulk and amorphous boron film samples, respectively [20]. The films were produced by sputtering crystalline boron on a quartz surface at 300°C-350°C with a resulting film thickness less than 1 μm. The mobility at room temperature was 2.2×10^{-1} cm²/Vs while the concentration of the carriers was not determined.

- In [21], a bulk amorphous boron sample was measured and the conductivity was equal to 7.6 $\times10^{-5}$ S/cm. The measured mobility was in the range of 1×10^{-2}-1×10^{-3} cm²/Vs, while the doping concentration was assumed to be approximately 10^{16} cm^{-3}.

- Samples prepared by plasma assisted chemical vapor deposition from boron trichloride gas (BCl$_3$) were only amorphous to some extent since high temperatures of 700°C-900°C caused the crystallization of the samples to α-rhombohedral boron [17]. The measured Hall mobility was between 5×10^{-3} and 10^{-1} cm²/Vs while the hole concentration was measured to be between 10^{16} and 10^{18} cm^{-3} [17].

- Time-of-flight measurements were performed on boron samples with thicknesses between 1.2 μm and 1.6 μm deposited on a silicon surface by an electron-beam evaporation technique [24]. Substrate temperatures were 200°C, 300°C and 350°C. From the measurements, hole drift mobility values between 5×10^{-2} and 5×10^{-1} cm²/Vs were extracted while the electron drift mobility was 3×10^{-1} cm²/Vs at room temperature. The mobility decreased with decreasing temperature which was explained by variable range hopping conduction.

Due to the difference in bandgap, amorphous boron should form a heterojunction when deposited on Si. In a simplified heterojunction model the band alignment between two semiconductor materials is determined by the electron affinity which can be modeled using Anderson's rule [25]. To the best of our knowledge, the electron affinity of amorphous boron material has not been reported in the literature. The electron affinity of the amorphous boron material could be extracted from measurements of the Schottky barrier height found for amorphous-boron metal systems and applying Schottky–Mott rule [25]. In [26], a gold electrode was contacted to amorphous boron films forming a Schottky contact with a barrier of 0.43 eV. The work function of gold is 5.1 eV [27] which gives an electron affinity of 4.67 eV. Significantly lower affinity can be extracted from a similar calculation based on the data of the Schottky barrier height of copper to hydrogenated amorphous boron [28]. The Schottky barrier height of a Cu/a-B:H interface was measured to be 0.8 ± 0.16 eV [28] while the copper work function is 4.7 eV [27]. The affinity of the a-B:H film can be calculated to be equal to 3.9 ± 0.16 eV. The same authors also reported the conduction and valence band offsets of the hydrogenated amorphous boron films to silicon in an a-B:H/Si configuration [29]. The conduction band offset of a-B:H/Si was found to be 0.15 ± 0.16 eV while the valence band offset of the a-B:H/Si heterojunction was equal to 0.15 ± 0.1 eV [29]. The conduction band offset variation led to the conclusion that the affinity of the a-B:H layer could be equal to the values measured for Si. In addition, the semiconductor work

function can also be used to construct a band diagram of a heterojunction knowing the position of the Fermi level. The semiconductor work function of polycrystalline boron was found to range from 4.3 eV to 4.45 eV for the photoelectric work function [27], [30]. If assumed that the Fermi energy is very close to the valence band edge which is specific to a highly-doped p-type semiconductor, one can find the affinity in the same range as calculated for the a-B:H films. The value of the effective density of states of boron is important for the calculation of the Fermi level energy inside the bandgap. The effective mass of holes in β-rhombohedral boron was found to be close to m_0 ($m_h^* \approx m_0$) [31] while the effective density of the valence states in amorphous boron is 10^{22} cm^{-3} [32].

An overview of the material properties of amorphous boron found in the literature is presented for both bulk-boron samples and samples where the boron is deposited in the form of a thin film. The properties are summarized in Table I.

III. ELECTRICAL MODELING

When contacted by p$^+$ implanted regions, PureB devices can achieve *I-V* characteristics comparable to conventional implanted p$^+$n junction in terms of low dark currents even for 1-nm thick PureB layers deposited at temperatures as low as 250°C [3]. From the past experimental PureB device results it appears that, when metallized, the PureB thickness does not play a role for the electron blocking effect if it is more than 2 nm and free of weak spots that were sometimes identified in connection with Si surface contamination before B deposition [3], [33]. The thickness does, however, present a significant series resistance if it exceeds the tunneling thickness of about 3 nm because the pure boron resistivity is > 500 Ω-cm [34]. Therefore, for advanced transistor applications it is desirable to have as thin as possible a layer. For very thin PureB layers less than 2 nm the electron injection current was seen to increase by decades, giving Schottky-like characteristics. Therefore, besides the effect of a negative fixed interface-charge, the influence of the metallization is also studied in the simulations.

A. Model parameters and all-Si simulations

For the simulations, Sentaurus Device [35] TCAD software was used. The basic all-Si test structure shown in Fig. 1 was simulated for varying thickness of the deposited top layer, t_{PB}, representing the PureB. The total thickness of the simulated n-type bulk-Si region was set at 500 μm with constant doping 10^{15} cm^{-3}. A fixed negative interface charge, N_I, was defined between the bulk-Si and the top-layer and varied between 10^{10} cm^{-2} and 5×10^{14} cm^{-2}. The
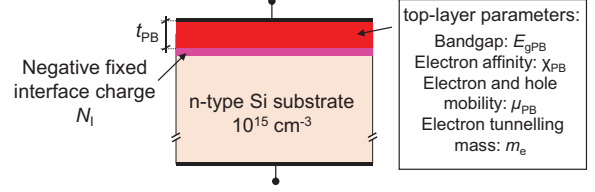

Fig. 1. Cross section of the simulated structure with indicated material parameters of the top layer.

doping of the top-layer, N_{PB}, was set to 10^{18} cm^{-3} as has been reported from experiments with amorphous boron [17]. Boron diffusion into Si is neglected. An Al-metal contact with a work function of 4.1 eV [35] was defined as contact to the top-layer. Band alignment and formation of the Al/top-layer barrier were chosen to follow the Schottky contact model [25] while Schottky-barrier height lowering was neglected. The thermionic emission model was simulated [36] and non-local tunneling to the anode contact was modeled [35] with tunneling mass for holes of $0.1\times m_0$, while tunneling mass for electrons, m_e, was varied from $0.1\times m_0$ to $0.8\times m_0$, where m_0 denotes the electron rest mass. Philips unified mobility model was applied [37]. Electron and hole concentrations are governed by Fermi-Dirac statistics. The material properties of the top-layer such as mobility of electrons and holes, μ_{PB}, bandgap, E_{gPB} and electron affinity, χ_{PB}, are individually varied from default Si-values to values typical for amorphous boron layers as indicated in Fig. 1.

The *I-V* characteristics of the all-Si structure were simulated and saturation current densities for electrons, I_{Se}, and holes, I_{Sh}, have been extracted for N_I between 10^{12} cm^{-2}

TABLE I. PROPERTIES OF AMORPHOUS BORON MATERIAL

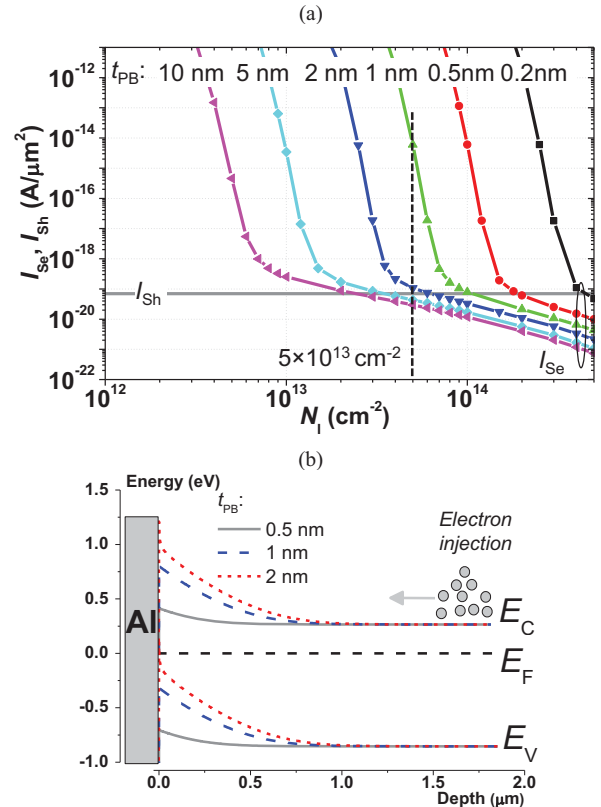|	Range	Reference
Bandgap	0.5 eV - 1.7 eV	[11]-[18]
Conductivity	10^{-3} S/cm - 10^{-5} S/cm	[13], [18]–[21]
Doping	≈3×10^{13} cm^{-3} - 10^{18} cm^{-3}	[17], [19], [21]
Mobility	1×10^{-3} cm^2/Vs - 10 cm^2/Vs	[17], [19]-[21], [24]
Affinity	4.67 eV; 3.9 ± 0.16 eV	[26], [28]

Fig. 2. (a) Electron and hole saturation current densities as a function of N_I extracted for a device with an Al/top-layer contact and t_{PB} = 0.2 nm, 0.5 nm, 1 nm, 2 nm, 5 nm and 10 nm. (b) Band diagram for N_I=5×10^{13} cm^{-2} and t_{PB} = 0.5 nm, 1 nm and 2 nm at V_D = 0 V.

and 5×10^{14} cm^{-2} and are shown in Fig. 2a. For the same concentration of negative interface charge, assuming an Al contact to the top layer causes band bending which lowers the barrier for electron injection as indicated in the band diagram shown in Fig. 2b. The distance between the Al contact and the PureB-Si interface, determined by the PureB layer thickness, dominates the accumulation of holes at the interface. Since the t_{PB} changes the concentration of holes at the interface, it is seen to have an impact on the built-in electric field and depletion region in Si. In the simulated all-Si test structure, suppression of electron injection from the bulk was achieved by introducing a large concentration of holes at the interface. The potential barrier formed in this way can lower the I_{Se} of the diode to become comparable to or lower than I_{Sh}.

B. Electron and hole mobility in the top-layer

Default mobility of carriers in the top-layer and the bulk Si was defined by the doping dependent Philips unified mobility model which resulted in an electron mobility of 65 cm^2/Vs and hole mobility of 44 cm^2/Vs for $N_{PB} = 10^{18}$ cm^{-3}. The mobility of holes in the top-layer was substituted for values found in the literature for amorphous boron material ranging from 10 cm^2/Vs to 10^{-3} cm^2/Vs [17], [19]–[21], [24]. For simplicity, the values of mobility for both the electrons and holes were defined to be the same, μ_{PB}, and were set to the values of 1 cm^2/Vs, 10^{-1} cm^2/Vs and 10^{-2} cm^2/Vs. The simulations were performed for devices with $t_{PB} = 1$ nm and 10 nm. Electron and hole tunneling masses are $0.1 \times m_0$. The electron and hole saturation current density as a function of N_I for both structures and all the mobility values are shown in Fig 3. For comparison, the I_{Se} of the device with the default Si mobility of the top-layer is also shown. The I_{Se} is the same irrespective of the mobility of the top-layer. The top-layer is thin and electron saturation current density is defined only by thermionic emission or tunneling through the barrier and the impact of the low mobility on the minority carrier diffusion can be neglected.

C. Electron affinity of the top-layer

PureB-Si represents a heterojunction and alignment of the two types of semiconductor materials depends on the affinity of each material as can be explained by Anderson's rule [25] which is used in the TCAD simulations. The exact affinity of the PureB material has not yet been measured, and the literature 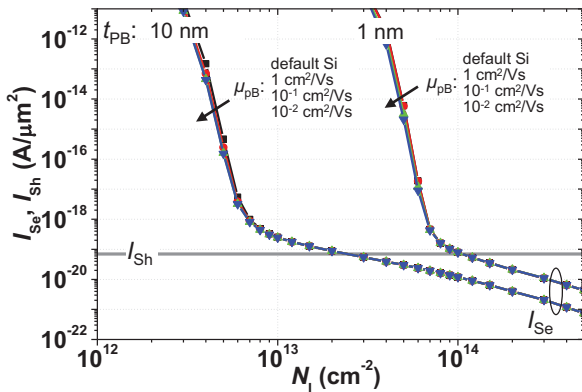sources do not report the affinity of any amorphous boron materials. The affinity of (hydrogenated) amorphous boron layers has been determined indirectly to vary in the range between 3.7 eV and 4.7 eV [26], [28] as discussed in Section II. Affinity of the top-layer, χ_{PB}, is therefore varied from default Si value which equals approximately 4.1 eV [35] to the values of 3.7 eV, 3.9 eV, 4.3 eV and 4.5 eV. The bandgap of top-layer is defined according to default Si value.

The simulations of I_{Se} and I_{Sh} for the devices with $t_{PB} = 1$ nm and 10 nm were performed and are shown as a function of N_I in Fig. 4a. Simulations are performed for $\chi_{PB} = 3.7$ eV, 3.9 eV, 4.1 eV, 4.3 eV and 4.5 eV while other parameters have default Si values. For devices with $t_{PB} = 10$ nm having the same N_I, the change of the affinity in the top-layer changes the shape of the barrier since the heterojunction formation impacts the concentration of electrons and holes in both the top-layer and near the top-layer/bulk-Si interface. The band diagram is plotted in Fig. 4b at $V_D = 0$ V for simulated structure with $t_{PB} = 10$ nm, $N_I = 2 \times 10^{13}$ cm^{-2} and χ_{PB} varied as: 3.7 eV, 4.1 eV and 4.5 eV. With an affinity of the top-layer lower than 4.1 eV, more holes are found in the top-layer region and a higher barrier is located in the top-layer. On the other hand, the hole concentration on the bulk-Si side of the interface decreases. The barrier in the bulk region also decreases which will allow higher injection of electrons. For χ_{PB} lower than 4.1 eV, larger N_I is needed to increase the barrier in the bulk-Si side to ensure the same blocking of the electron injection from the bulk. For $\chi_{PB} > 4.1$ eV more holes are generated at the bulk-Si side of the top-layer/bulk-Si interface and the barrier for the electron injection is roughly the same as for the default Si value of χ_{PB}.
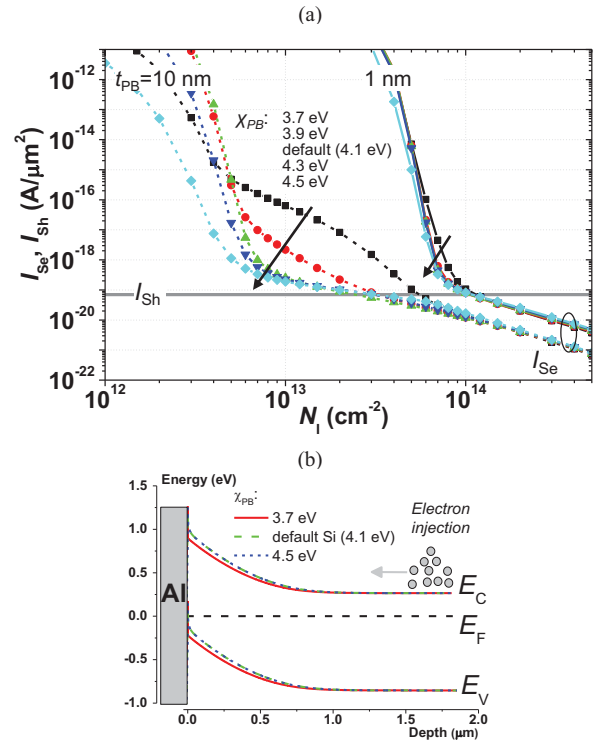
(a)

(b)

Fig. 4. (a) Electron and hole saturation current densities as a function of N_I extracted for a device with $t_{PB} = 1$ nm and 10 nm for the top-layer having electron affinity, χ_{PB}: 3.7 eV, 3.9 eV, 4.1 eV, 4.3 eV and 4.5 eV. (b) Band diagram at $V_D = 0$ V for the simulated structure with $t_{PB} = 10$ nm, $N_I = 2 \times 10^{13}$ cm^{-2} and χ_{PB}: 3.7 eV, 4.1 eV and 4.5 eV.

Fig. 3. Electron and hole saturation current densities as a function of N_I extracted for the device with $t_{PB} = 1$ nm and 10 nm for a top-layer having an electron and hole mobility: default for Si, 1 cm^2/Vs, 10^{-1} cm^2/Vs or 10^{-2} cm^2/Vs.
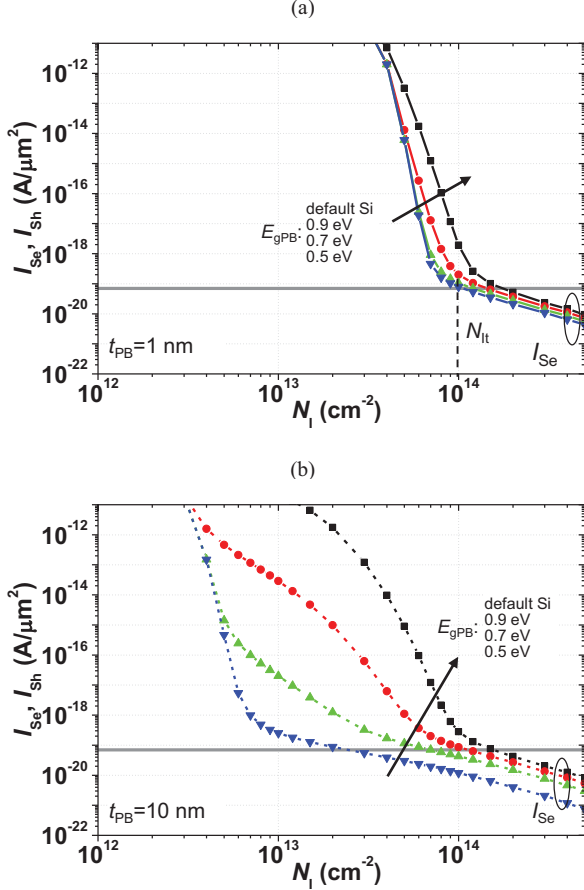
(a)

(b)

Fig. 5. Electron and hole saturation current densities as a function of N_I extracted for a device with: (a) t_{PB} = 1 nm; (b) t_{PB} = 10 nm. The bandgap of the top-layer is varied as: default Si value, 0.9 eV, 0.7 eV and 0.5 eV.

D. Bandgap of the top-layer

A change in the bandgap of the top-layer, E_{gPB}, causes a discontinuity at the interface which will change the hole concentration near the top-layer/bulk-Si interface. The impact of the bandgap change on the suppression of electron injection was simulated. The simulation results for I_{Se} and I_{Sh} as a function of N_I of the structure with t_{PB} = 1 nm are shown in Fig 5a and for t_{PB} = 10 nm in Fig 5b. All other material parameters have their default values. The N_I needed to decrease I_{Se} to values below I_{Sh} was designated as N_{It}. For t_{PB} = 1 nm, N_{It} increases from 1×10^{14} cm^{-2} for the default Si bandgap of the top-layer to the values of 1.8×10^{14} cm^{-2} for E_{gPB} = 0.5 eV. For t_{PB} = 10 nm the difference in N_{It} is even larger and N_{It} increases from 2.4×10^{13} cm^{-2} for the default Si bandgap of the top-layer to values of 1.6×10^{14} cm^{-2} for E_{gPB} = 0.5 eV. The band diagram at V_D = 0 V for the structure with t_{PB} = 10 nm having N_I =
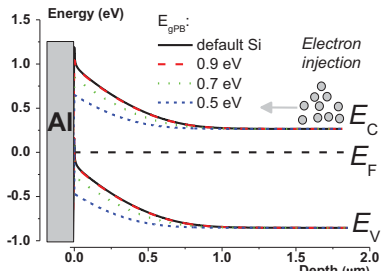

Fig. 6. Band diagram at V_D = 0 V for the simulated structure with t_{PB} = 10 nm, N_I = 2×10^{13} cm^{-2} and E_{gPB}: the same as in Si ($\approx$1.1 eV), 0.9 eV, 0.7 eV and 0.5 eV.

2×10^{13} cm^{-2} is shown in Fig. 6 for varied bandgap of the top-layer as listed in the figure. For low E_{gPB}, the bulk-Si near the top-layer/bulk-Si interface can be completely depleted of holes. The decrease of the bandgap will reduce the barrier seen by the electrons injected from the bulk. Therefore, the N_I needed to set the same potential barrier for suppressing the electron injection will be higher if the top-layer has a bandgap narrower than the default Si value.

E. Electron tunneling mass

Besides the material parameters of the top-layer, the tunneling mass of the electrons also affects the I_{Se} of the diode. The default values for both the electron and hole tunneling masses were the same in the top-layer and in the bulk-Si and by default equal $0.1 \times m_0$. When the barrier for electrons, formed by the negative fixed charge, is sufficiently high, the carriers can only be transported through the barrier by tunneling. Increasing the electron tunneling mass will lower the tunneling probability and I_{Se} will decrease. The impact of the electron tunneling mass on the electron saturation current density of the test structure was simulated and the results for t_{PB} = 1 nm and 10 nm are shown in Fig. 7. The electron tunneling mass was varied as $0.1 \times m_0$, $0.3 \times m_0$, $0.5 \times m_0$ and $0.8 \times m_0$. All other material parameters were set to the default Si values. The tunneling component of the electron current starts to dominate the I_{Se} for values lower than 10^{-18} A/μm^2 and it does not affect the critical concentration of the negative fixed charge needed to lower I_{Se} below I_{Sh}. The hole tunneling does not affect electron injection suppression and is only important for transport of holes from the contact to the interface. Most probably, tunneling is governed by VRH conduction characteristic to amorphous materials [23]. However, modeling of VRH is not supported by TCAD simulations. To this end, tunneling of holes is simulated by assuming a constant hole tunneling mass.

IV. CONCLUSIONS

The rectifying behavior of junctions formed by PureB deposition is suspected to come from PureB-Si interface where negative fixed charge is responsible for the accumulation of holes. The thus formed barrier then stops injection of electrons from the Si bulk lowering the dark current of diodes where the PureB layer is deposited in the anode region. The simulation study presented in this paper confirms that a concentration of fixed negative charge
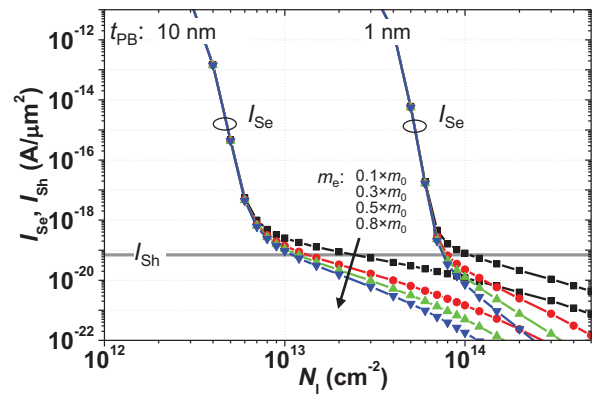

Fig. 7. Electron and hole saturation current densities as a function of N_I extracted for a device with t_{PB} = 1 nm and 10 nm for the electron tunneling mass of: $0.1 \times m_0$, $0.3 \times m_0$, $0.5 \times m_0$ and $0.8 \times m_0$.

could be responsible for low saturation current densities of PureB diodes if it is high enough. Material properties of the boron layer may considerably vary with deposition conditions and most of the PureB material parameters are not well-known. An investigation where a large number of material parameters of the ultra-thin layer were varied was performed to gain insight into effectiveness of the barrier formed by the negative fixed interface charge. The variations in affinity, mobility, electron tunneling mass, and bandgap all confirmed that a critical concentration of negative fixed charge is needed to lower the I_{Se} below the I_{Sh}. Depending on the thickness of the layer, effective suppression of electron injection is achieved for N_I from $\approx 10^{13}$ cm^{-2} to $\approx 2\times10^{14}$ cm^{-2}.

REFERENCES

[1] K.-S. Kim *et al.*, "A novel doping technology for ultra-shallow junction fabrication: boron diffusion from boron-adsorbed layer by rapid thermal annealingq," *Thin Solid Films*, p. 6, 2000.

[2] E. Y.-J. Kong, P. Guo, X. Gong, B. Liu, and Y.-C. Yeo, "Toward Conformal Damage-Free Doping With Abrupt Ultrashallow Junction: Formation of Si Monolayers and Laser Anneal as a Novel Doping Technique for InGaAs nMOSFETs," *IEEE Transactions on Electron Devices*, vol. 61, no. 4, pp. 1039–1046, Apr. 2014.

[3] T. Knežević, X. Liu, E. Hardeveld, T. Suligoj, and L. K. Nanver, "Limits on thinning of boron layers with/without metal contacting in PureB Si (photo)diodes," *IEEE Electron Device Letters*, preprint, 2019.

[4] J. F. Dick, A. Elsayed, D. Schwarz, and J. Schulze, "Electrical characterization of low-temperature boron on silicon deposition utilizing molecular beam epitaxy," in *MIPRO, 2019 Proceedings of the 42nd International Convention*, 2019.

[5] F. Sarubbi, L. K. Nanver, T. L. M. Scholtes, S. N. Nihtianov, and F. Scholze, "Pure boron-doped photodiodes: a solution for radiation detection in EUV lithography," in *ESSDERC 2008-38th European Solid-State Device Research Conference*, 2008, pp. 278–281.

[6] A. Šakić *et al.*, "Versatile silicon photodiode detector technology for scanning electron microscopy with high-efficiency sub-5 keV electron detection," in *Electron Devices Meeting (IEDM), 2010 IEEE International*, 2010, pp. 31–4.

[7] L. Qi, K. R. C. Mok, M. Aminian, E. Charbon, and L. K. Nanver, "UV-Sensitive Low Dark-Count PureB Single-Photon Avalanche Diode," *IEEE Transactions on Electron Devices*, vol. 61, no. 11, pp. 3768–3774, Nov. 2014.

[8] L. K. Nanver *et al.*, "Pure Dopant Deposition of B and Ga for Ultrashallow Junctions in Si-based Devices," *ECS Transactions*, vol. 49, no. 1, pp. 25–33, Aug. 2012.

[9] L. K. Nanver *et al.*, "Robust UV/VUV/EUV PureB Photodiode Detector Technology With High CMOS Compatibility," *IEEE Journal of Selected Topics in Quantum Electronics*, vol. 20, no. 6, pp. 306–316, Nov. 2014.

[10] L. Qi and L. K. Nanver, "Conductance Along the Interface Formed by 400 °C Pure Boron Deposition on Silicon," *IEEE Electron Device Letters*, vol. 36, no. 2, pp. 102–104, Feb. 2015.

[11] J. P. Schaffer, H. Park, J. H. Lind, and P. L. Jones, "Hydrogenated Amorphous Boron: Transient and Steady State Photoconductivity," *physica status solidi (a)*, vol. 81, no. 1, 1984.

[12] F. H. Cocks, P. L. Jones, and L. J. Dimmey, "The optical band gap of hydrogenated amorphous-boron thin films: The effect of thermal treatment," *Applied Physics Letters*, vol. 36, no. 12, pp. 970–972, Jun. 1980.

[13] Y. Kumashiro, T. Yokoyama, J. Nakahura, K. Hatsuda, H. Yoshida, and J. Takahashi, "Thermoelectric Properties of Boron and Boron Phosphide Film," in *MRS Proceedings*, 1992, vol. 242, p. 629.

[14] U. Kuhlmann, H. Werheit, T. Lundström, and W. Robers, "Optical properties of amorphous boron," *Journal of Physics and Chemistry of Solids*, vol. 55, no. 7, pp. 579–587, 1994.

[15] A. Hori, M. Takeda, H. Yamashita, and K. Kimura, "Absorption Edge Spectra of Boron-Rich Amorphous Films Constructed with Icosahedral Cluster," *Journal of the Physical Society of Japan*, vol. 64, no. 9, pp. 3496–3505, Sep. 1995.

[16] O. Madelung, U. Rössler, and M. Schulz, Eds., *Non-Tetrahedrally Bonded Elements and Binary Compounds I*, vol. 41C. Berlin/Heidelberg: Springer-Verlag, 1998.

[17] K. Kamimura, M. Ohkubo, T. Shinomiya, M. Nakao, and Y. Onuma, "Preparation and properties of boron thin films," *Journal of Solid State Chemistry*, vol. 133, no. 1, pp. 100–103, 1997.

[18] A. A. Berezin *et al.*, "Electrical and optical properties of amorphous boron and amorphous concept for ß-rhombohedral boron," *Journal of Non-Crystalline Solids*, vol. 16, no. 2, pp. 237–246, Nov. 1974.

[19] K. Kumashiro *et al.*, "Thermoelectric Properties of Boron and Boron Phosphide Films," *Journal of Solid State Chemistry*, vol. 154, no. 1, pp. 26–32, Oct. 2000.

[20] O. A. Golikova, "Amorphous boron films with enhanced electrical conductivity," *Semiconductors*, vol. 34, no. 3, pp. 363–366, 2000.

[21] Y. Kumashiro, T. Yokoyama, and Y. Ando, "Thermoelectric properties of boron and boron phosphide CVD wafers," in *Thermoelectrics, 1998. Proceedings ICT 98. XVII International Conference on*, 1998, pp. 591–594.

[22] Y. Wang, R. J. Hamers, and E. Kaxiras, "Atomic structure and bonding of boron-induced reconstructions on Si (001)," *Physical review letters*, vol. 74, no. 3, p. 403, 1995.

[23] N. F. Mott, "Conduction in non-crystalline materials: III. Localized states in a pseudogap and near extremities of conduction and valence bands," *Philosophical Magazine*, vol. 19, no. 160, pp. 835–852, Apr. 1969.

[24] M. Takeda, K. Kimura, and K. Murayamat, "Transient Photocurrent Studies on Amorphous and ß-Rhombohedral Boron," 1997.

[25] S. M. Sze and K. K. Ng, *Physics of Semiconductor Devices*, 3rd edition. Hoboken, N.J: Wiley-Interscience, 2006.

[26] G. Caserta and A. Serra, "Electrode-limited conduction in amorphous boron films IDC measurements," *Thin Solid Films*, vol. 20, no. 1, pp. 91–101, 1974.

[27] H. B. Michaelson, "The work function of the elements and its periodicity," *Journal of Applied Physics*, vol. 48, no. 11, pp. 4729–4733, Nov. 1977.

[28] S. W. King *et al.*, "Valence band offset and Schottky barrier at amorphous boron and boron carbide interfaces with silicon and copper," *Applied Surface Science*, vol. 285, pp. 545–551, Nov. 2013.

[29] S. W. King, M. French, M. Jaehnig, M. Kuhn, and G. Xu, "Valence Band Offset at aB:H and a-BP:H/Si Interfaces," *ECS Journal of Solid State Science and Technology*, vol. 1, no. 5, pp. P250–P253, 2012.

[30] B. Seroczyńska-Wojas, "Photoemission from beta-rhombohedral boron," *Physica Status Solidi (a)*, vol. 30, no. 1, pp. K73–K76, Jul. 1975.

[31] O. A. Golikova, "Boron and Boron-based semiconductors," *physica status solidi (a)*, vol. 51, no. 1, pp. 11–40, 1979.

[32] G. P. Tsiskarishvili, G. V. Tsagareishvili, M. E. Antadze, and F. N. Tavadze, "Nature of Paramagnetic Centers in Amorphous Boron," *MRS Proceedings*, vol. 97, Jan. 1987.

[33] X. Liu, L. K. Nanver, and T. L. M. Scholtes, "Nanometer-Thin Pure Boron Layers as Mask for Silicon Micromachining," *JOURNAL OF MICROELECTROMECHANICAL SYSTEMS*, vol. 26, no. 6, pp. 1428–1434, Dec. 2017.

[34] V. Mohammadi, S. Ramesh, and L. K. Nanver, "Thickness evaluation of deposited PureB layers in micro-/millimeter-sized windows to Si," in *Microelectronic Test Structures (ICMTS), 2014 International Conference on*, 2014, pp. 194–199.

[35] Synopsys, *Sentaurus Device User Guide Version N-2017.09*. Mountain View, CA, USA: Synopsys, 2017.

[36] D. Schroeder, *Modelling of Interface Carrier Transport for Device Simulation*. Vienna: Springer Vienna, 1994.

[37] D. B. M. Klaassen, "A unified mobility model for device simulation—I. Model equations and concentration dependence," *Solid-State Electronics*, vol. 35, no. 7, pp. 953–959, Jul. 1992.